Regional Cerebral Blood Flow in Mood Disorders. II. Comparison of Major Depression and Alzheimer's Disease

Harold A. Sackeim, Isak Prohovnik, James R. Moeller, Richard Mayeux, Yaakov Stern and D. P. Devanand

Department of Biological Psychiatry, New York State Psychiatric Institute and the Departments of Neurology, Psychiatry, and Radiology, College of Physicians and Surgeons, Columbia University, New York, New York

We contrasted regional cerebral blood flow in matched groups of 30 patients with major depression, 30 patients with Alzheimer's disease and 30 normal controls using the ^{133}Xe inhalation technique. Whereas both the depressed and Alzheimer's disease groups had markedly reduced global cortical blood flow, the Scaled Subprofile Model, developed to identify abnormalities in regional networks, indicated that they had distinct topographic profiles. Previous findings of an abnormal regional network in major depression were unaltered by the inclusion of Alzheimer's disease patients in the analysis. Alzheimer's disease was associated with a distinct parietotemporal deficit and the degree of this abnormality strongly covaried with cognitive impairment. Alzheimer's disease patients also had abnormal manifestation of three other regional networks. We illustrate a method for distinguishing when a disease imposes a new pattern of interactions among brain regions and when a disease alters the expression of regional patterns characteristic of normal functioning.

J Nucl Med 1993; 34:1090–1101

Differentiating Alzheimer's disease (AD) from major depression (MD), while crucial for treatment planning, is at times difficult (1,2). Only 80% of antemortem AD diagnoses may be validated by neuropathological findings (3–5) and some elderly depressed patients have marked cognitive impairment (6,7). It has been suggested that AD and MD may each be associated with distinct topographic abnormalities of cerebral blood flow (CBF) and metabolism (8,9). However, there has yet to be extensive, direct comparison of these conditions using functional imaging techniques (10).

A large number of studies have demonstrated that AD is associated with a global cortical reduction in blood flow and metabolism (11–14), as well as a characteristic deficit in parietotemporal cortex, with relative preservation in calcarine and sensorimotor regions (15–19). There is evidence that the global cortical reductions in blood flow and metabolism correlate with the extent of cognitive impairment in AD (11,17,20–22) and this covariation may be most strongly manifested in the parietotemporal cortex (19,23,24). Some investigators have also reported reduced functional activity in the frontal cortex, although typically to a lesser extent than in parietotemporal regions (22,25,26). In addition, disturbed patterns of lateralized metabolic activity characterize a subgroup of AD patients, with the direction of lateralized abnormalities correlating with patterns of neuropsychological deficit (27–29).

Imaging studies in depressed patients have observed a variety of abnormalities including reductions in blood flow or metabolism globally and in selective frontal, temporal, parietal and subcortical regions (30–39). Some investigators have emphasized frontal cortex abnormalities in MD and have suggested that findings of a pronounced parietotemporal deficit should favor an AD diagnosis, whereas a pattern of parietotemporal preservation with frontal cortex deficit may indicate MD (9,10). However, this inference is questionable. First, in the bulk of previous imaging studies, MD samples have been relatively young patients with only mild to moderate symptomatology. For comparison with AD, samples of elderly and severely depressed patients are of greater relevance. Second, a focus on frontal cortex abnormalities would likely provide an incomplete view of the topographic deficits in MD.

It has been increasingly recognized that complex psychological phenomena are subserved by networks of spatially distributed brain regions (40–42). These intrinsic networks, defined as patterns of covariance among brain regions, may not correspond to the spatial organization frequently imposed on brain imaging data. A common approach to identifying topographic abnormalities has been to average values in anatomically adjacent regions into groupings by lobe (33,43,44) or brain quadrant (e.g., left and right anterior and posterior) (45,46). Besides reducing spatial resolution, such transformations presume that there are greater functional interrelations or covariance among the regions within a grouping than between regions represented in different groupings and contradict the view that functional networks may have wide spatial distribution.

TABLE 1
Demographic and Physiologic Correlates of CBF in Normal Controls and Patients with Major Depression or Alzheimer's Disease

	Normal controls	Major depression	Alzheimer's disease
	10 M, 20 F	11 M, 19 F	13 M, 17 F
Age (yr)	64.30 ± 8.61	65.57 ± 7.15	67.40 ± 8.90
PCO_2 (mmHg)	37.92 ± 3.02	38.08 ± 4.97	38.62 ± 4.02
Systolic BP (mmHg)	133.50 ± 16.51	131.80 ± 20.91	139.75 ± 21.23
Diastolic BP (mmHg)	81.40 ± 10.16	81.27 ± 11.57	83.18 ± 12.33

BP = blood pressure.

Consequently, the identification that a clinical sample has a deficit in an a priori grouping of brain regions neither ensures that the topographic deficit provides an exhaustive description of the abnormal network nor does it guarantee that the deficit is consistent within the grouping.

These and related problems were illustrated in a previous paper in this series (47). By using the ^{133}Xe technique to measure regional cerebral blood flow (rCBF), we contrasted matched groups of relatively elderly MD patients and normal controls, applying both conventional multivariate statistical techniques and the Scaled Subprofile Model (SSM) that was developed to identify abnormal functional networks in clinical samples (48). The depressed group had a marked global reduction in CBF, as well as a specific topographic deficit. By SSM, the topographic deficit in the MD group was due to CBF reductions in selective frontal, central, superior temporal and anterior parietal regions. This pattern appeared to correspond to the parallel distributed network of prefrontal and parietotemporal polymodal association areas that had been implicated in arousal, attentional and motivational functions, as well as representational cognitive processes (42,49–51). Within the MD group, abnormality in this network increased both as a function of patient age and severity of depressive symptoms.

Our previous findings that MD was associated with a global reduction in cortical CBF and with a topographic deficit involving selective frontal, temporal and parietal regions raised concern about the specificity of the deficits in MD as compared to AD. Here, we examine whether these conditions are associated with distinct topographic abnormalities. A second aim was to investigate the reliability and validity of SSM. Since it is already established that AD is associated with a characteristic parietotemporal deficit, we sought to determine: (1) whether an abnormal network corresponding to a parietotemporal deficit would emerge when adding a sample of AD patients to the previously studied MD and normal control samples, (2) whether the severity of cognitive impairment within the AD patients covaried with manifestation of such a network abnormality

and (3) whether the previously determined network abnormality in major depression was stable or altered by the inclusion in the blind SSM analysis of a patient sample with known and possibly distinct topographic disturbance.

MATERIALS AND METHODS

Patient Population

The study cohort comprised 30 AD, 30 MD and 30 normal controls. The MD and normal subjects were selected blind to rCBF results from the larger, previously reported samples of 41 MD and 40 controls to create equally-sized groups matched on the mean, variance and shape of distributions of age, end-tidal PCO_2 and systolic and diastolic blood pressure and the distribution of gender (Table 1). The MD patients met the Research Diagnostic Criteria (52) for major depressive disorder and endogenous subtype using the Schedule for Affective Disorders and Schizophrenia (53). Participation required a score of 18 or greater on the Hamilton Rating Scale for Depression (HRSD) (54). Exclusion criteria have been previously reported (47). Laboratory tests (urinalysis, SMA20, CBC, thyroid function) and chest roentgenogram were within normal limits. With the exception of low doses of lorazepam, the MD sample was withdrawn from psychotropic medication at least 5 days before rCBF measurement. The mean (±s.d.) psychotropic washout was 12.73 ± 6.11 days (median, 10 days), with an upper limit of 28 days taken for longer drug-free periods. No lorazepam was administered within 10 hr of the measurement. The average lorazepam dose 24 hr before rCBF assessment was 0.99 ± 0.79 mg (range 0–3.0 mg). Length of medication washout and the presence, absence or dosage of lorazepam were not associated with CBF parameters. The normal controls were paid volunteers who were negative for psychiatric and neurologic history. None had taken prescription or nonprescription medication for at least 2 wk before rCBF measurement.

The AD sample met DSM-III criteria for primary degenerative dementia at durations of illness for less than 1 yr and NINCDS-ADRDA criteria (3) for probable Alzheimer's disease at durations of 1 yr or longer. These outpatients underwent comprehensive neurological, CT, EEG, neuropsychological examinations and MRI and cerebrospinal fluid studies, if indicated. Laboratory tests were within normal limits. All AD patients were negative for the presence of major depression, delusions or hallucinations and had negative psychiatric histories. They were free of psychotropic medication for at least 1 mo prior to rCBF measurement. Of the 30 AD patients, 27 had been included in a previously reported sample of 36 patients (55). Patients were excluded from this study due to incomplete rCBF data (n = 2), concurrent medication, psychiatric history (n = 5) or to produce adequate matching of the groups (n = 2). Three newly studied AD patients were added to achieve comparable sample sizes.

The modified Mini-State examination (mMMS, total possible score of 57) was used to quantify the severity of global cognitive impairment (56,57). Capacity to conduct activities of daily life was assessed with the first part of the Blessed Dementia Rating Scale (BDRS) (58). The AD sample was weighted with cases of short illness duration (mean = 3.06 yr, s.d. = 1.77, range = 0.75–6 yr) and relatively mild to moderate cognitive impairment (mean mMMS = 30.80, s.d. = 14.61, range, 0–53) and functional incapacity (mean BDRS = 7.72, s.d. = 3.04, range, 3–14). All 90 subjects were right handed.

TABLE 2
Descriptive Statistics and ANCOVA Results for Global CBF Values

Variable	Normal control mean ± s.d.	Major depression mean ± s.d.	Alzheimer's disease mean ± s.d.	F-test		
				Group	Sex	Group x sex
M2 ISI	49.06 ± 7.00	43.01 ± 6.84	41.36 ± 6.29	12.78‡	4.68*	0.25
M2 f_g	63.54 ± 9.55	55.68 ± 10.25	54.96 ± 8.30	8.67‡	2.12	0.14
M1 ISI	51.72 ± 6.45	46.55 ± 6.64	45.10 ± 6.94	9.97‡	4.78*	0.53
M1 f_g	66.58 ± 7.03	60.96 ± 8.78	62.08 ± 8.17	4.77†	5.24*	0.02
M2 CBF15	39.20 ± 5.92	34.87 ± 5.28	33.17 ± 4.75	12.07‡	3.13	0.32
M2 k_2	0.11 ± 0.01	0.10 ± 0.02	0.10 ± 0.02	7.11‡	0.44	0.05
M2 w_g, %	40.54 ± 4.45	40.07 ± 3.98	37.71 ± 4.03	3.92*	0.90	0.24

*$p < 0.05$.
†$p < 0.01$.
‡$p < 0.001$.

M2 = six-unknown model used to determine flow parameters; M1 = the four-unknown model; ISI = initial slope index; f_g = fast compartment, gray-matter flow rate (in ml per 100 g per min); CBF15 = flow rate in all perfused tissue; k_2 = slow compartment, white matter clearance; and w_g = relative weight of gray matter to total perfused tissue.

rCBF Measurement

Procedures for rCBF measurement have been previously detailed (47). Assessments were made under resting, supine conditions in a quiet, darkened room with weighted blinders placed over the eyes. A commercial device (Novo Cerebrograph 32c, Copenhagen, Denmark) was used with head positioning established by determining the orientation of a helmet housing 32 scintillation detectors (16 per hemisphere) in relation to light markers aligned to the canthomeatal line. Extensive quality control procedures were used as detailed elsewhere (59). End-tidal PCO_2 was monitored during the 11-min measurement period and blood pressure was determined following the measurement. Clearance curves were analyzed both with a six-unknown model (M2), which provides greater sensitivity under low flow conditions and more accurate artifact removal, and the traditional four-unknown model (M1) (60,61). The major dependent variable was the M2 initial slope index (M2 ISI) (62). The statistical analysis procedures are described in the Appendix.

RESULTS

The three groups were equivalent in the distribution of gender (Table 1). ANOVAs (grouped by sex) indicated that the groups were also equivalent in age, end-tidal PCO_2 and blood pressure values. There was a main effect of sex on age ($p = 0.01$), with females (mean ± s.d., 67.38 ± 7.71) being older than males (63.09 ± 8.57), a pattern manifested in all three groups. No other main effect or interaction was significant. Across the groups, global flow was higher in females than in males ($p < 0.02$), despite the age difference. Global flow positively correlated with PCO_2 ($r = 0.33$, $p < 0.002$).

Global Flow Effects

As seen in Table 2, the ANCOVAs on global values yielded a main effect of group for every CBF parameter. With the exception of M2 w_g, both the MD and AD groups for each parameter had significantly lower values than normal controls but did not differ from each other. The MD and AD groups had marked and equivalent global reductions in both gray matter flow (f_g) and white-matter clear-

ance (k_2). M2 w_g is an anatomic index, assessing the relative amount of fast-clearing tissue (gray matter) relative to total perfused tissue. The groups also differed significantly in w_g, with post hoc comparisons indicating that the AD group had reduced w_g relative to both the MD group ($p < 0.05$) and normal controls ($p < 0.01$), with no difference between the latter two groups. This suggested a loss of cortical gray matter in the AD group (63). The group differences in cell loss did not influence the global or regional CBF measures. Unlike most applications of PET or SPECT (64) with agents that remain fixed intracellularly, the ^{133}Xe technique quantifies CBF only in perfused tissue.

Global and Topographic Abnormalities: SSM

The terms and procedures involved in the SSM analysis are defined in the Appendix. In applying SSM to the M2 ISI values, four topographic structures (GISs) were identified that accounted for 49% of the subject by region variance (SRPs). Individual differences in manifesting these topographic patterns (SSFs) accounted for 23% of the variance in raw global CBF. Therefore, a substantial portion of the variability in global CBF was due to topographic effects. To determine SSM's parameter of a region-independent global value (GSF), the contributions of these four topographic patterns to raw global values was removed.

The mean GSF (in ISI units) was 46.42 ± 6.74 for normal controls, 42.97 ± 7.06 for the MD group and 43.48 ± 5.72 for the AD group. An ANCOVA on GSF values yielded a significant effect of the PCO_2 covariate ($p = 0.002$) and a trend for a main effect of group ($p = 0.09$). The MD patients had significantly lower GSF values than controls ($p = 0.03$), while AD patients tended to have lower values than controls ($p = 0.08$). The differences among the groups in SSM's estimate of global flow were smaller than the differences observed in raw global flow. This was because in both patient groups the deficits in raw global flow were due to a combination of diffuse and focal abnormalities. SSM removes focal effects in estimating the GSF.
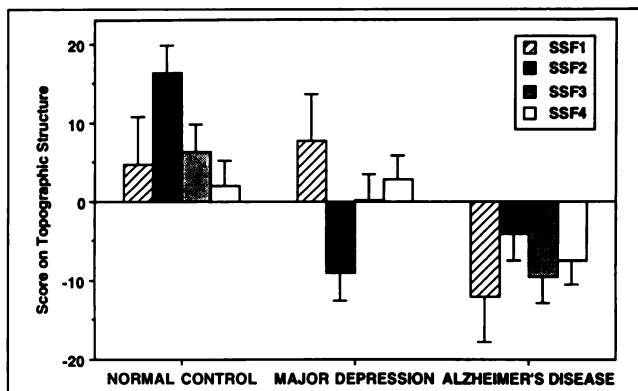
FIGURE 1. Mean (±s.e.) values for the three groups in manifesting each of four topographic patterns identified with the SSM. SSF = subject scaling factor.

Figure 1 presents the mean scores of the three groups on the four topographic structures. A repeated measures MANCOVA was conducted on these scores (SSFs). There was a main effect of the group (p = 0.01) and an interaction between the group and topographic structure (p < 0.0001). There was also an interaction between sex and topographic structure (p = 0.02) indicating gender differences in topography. To determine the source of the significant multivariate effects of the diagnostic group, follow-up ANCOVAs were conducted on each SSF. In all analyses, the main effect of the group was significant (SSF1: p < 0.05; SSF2: p < 0.0001; SSF3: p < 0.005; SSF4: p < 0.05). The AD group differed from normal controls in manifesting each of the four topographic structures (0.05 > p > 0.0005). The MD group differed from normal controls only in SSF2 (p < 0.0001). The MD and AD groups differed in manifesting three of the four topographic patterns (SSF1: p < 0.02; SSF3: p < 0.05; SSF4: p = 0.02).

Table 3 presents the regional covariance patterns described by each GIS. For this study, the signs of the region weights in Table 3 were oriented so that negative values reflect regions of relative flow deficit in the clinical groups. The first topographic structure defined a clear anterior-posterior dimension, characterized by relatively higher anterior than posterior CBF. The MD and normal controls were equivalent in this pattern of 'hyperfrontality.' Compared to both these groups, the AD sample had exaggerated 'hyperfrontality,' due to posterior flow deficits. The second structure described the only abnormal topography in the MD group. As shown in Figure 2, this deficit corresponded to reductions in selective frontal, central, superior temporal and anterior parietal regions. Only the AD group had abnormal manifestation of the third topographic structure, which is also illustrated in Figure 2. This covariance pattern closely conformed to the classic parietotemporal deficit previously reported in AD. It involved flow deficits in bilateral temporal and parietal regions with a somewhat greater involvement of the left than right temporal areas. The last structure reflected patterns of asymmetry. The AD group was also abnormal in displaying this pattern which was characterized by relatively higher right than left CBF in selective frontal and parietal regions in the normal controls and MD patients.

Stability of SSM Parameters

Compared to our previous report (47), the findings obtained here involved blindly excluding 11 MD and 10 control subjects and introducing 30 AD patients. We examined the stability of the identification of regional networks across the two studies and determined which topographic pattern newly emerged with the introduction of AD patients. Previously, three topographic structures had been

TABLE 3
Region Weights on Four Topographic Structures (GISs)*

Region	GIS1	GIS2	GIS3	GIS4	Region	GIS1	GIS2	GIS3	GIS4
	Left hemisphere					Right hemisphere			
F1	*0.46*	**−2.89**	−2.79	−3.24	F1	−0.19	**−3.89**	−1.90	**−5.35**
F2	−0.88	**−3.35**	−2.63	−1.70	F2	−0.37	**−3.20**	−1.19	−3.10
F3	*0.49*	−2.37	−2.73	−2.06	F3	*0.47*	**−2.74**	−2.32	**−3.40**
F4	*0.00*	−2.64	−3.03	−1.34	F4	*0.03*	**−3.05**	−2.02	−2.54
F5	*−0.14*	−1.80	−2.40	−1.77	F5	−0.21	−2.46	−1.70	−2.22
C1	−0.73	−1.56	−2.43	−1.67	C1	−0.98	−1.93	−1.29	−2.11
C2	−0.57	**−2.83**	−2.05	−1.92	C2	−0.66	−2.64	*−0.56*	−1.59
T1	*1.83*	0.01	−3.70	**−3.49**	T1	*1.90*	−0.01	−2.93	−3.20
T2	−0.61	−2.39	**−3.18**	*−1.53*	T2	−0.30	**−2.85**	−2.99	*−1.18*
T3	−1.07	*−1.17*	−1.75	*−1.20*	T3	−1.51	*−0.44*	−2.13	*−1.28*
P1	−1.87	**−2.82**	**−4.59**	−2.55	P1	−1.75	−2.52	**−3.72**	−3.19
P2	−1.62	−1.43	**−4.23**	−2.89	P2	−1.81	−1.95	**−3.14**	**−3.44**
P3	**−1.38**	−1.88	**−3.84**	−2.72	P3	**−1.30**	−1.82	**−3.16**	**−3.95**
P4	**−1.93**	*−1.11*	−1.99	−2.90	P4	**−1.34**	−1.24	*−0.96*	**−3.79**
O1	**−1.64**	−1.24	**−3.52**	−2.63	O1	**−1.96**	−1.74	−2.08	−3.17
O2	−0.97	*−0.25*	−1.37	−2.08	O2	**−1.61**	*−0.89*	*−0.91*	**−4.32**

*The AD group was abnormal in manifesting all four networks and the MD group had abnormal values on GIS2. Negative values indicate regions of relative flow deficit. Values in bold are significant in specifying the abnormal cerebral blood flow patterns and define the network; italicized weights do not participate in the network and are regions of relatively preserved flow.
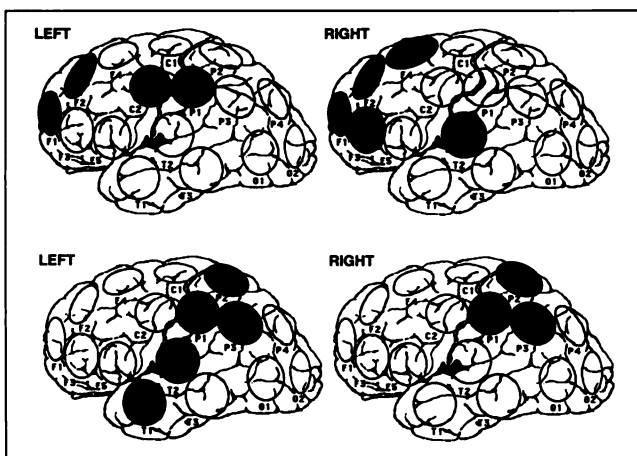
FIGURE 2. (Top) The second topographic structure identified by the SSM. The only topographic abnormality in patients with major depression was in this profile. Darkened regions were areas that significantly participated in this network and defined the topographic blood flow deficits in major depression. (Bottom) The third topographic structure identified by the SSM. This parietotemporal pattern was introduced by patients with AD and the extent to which these patients manifested deficits in this pattern correlated strongly with their degree of cognitive impairment. Relative orientation of the detectors in the helmet is denoted by shape. F = frontal; C = central; T = temporal, P = parietal; O = occipital.

identified in contrast to the four patterns obtained here. In both studies, the first structure (GIS1) described an anterior-posterior dimension. The correlation was nearly perfect between the weights of the 32 regions in the structure identified here and in our previous report ($r = 0.94$, $p < 0.0001$). The correlation in scores for manifesting this topography (SSF1) for the 60 subjects (30 MD and 30 controls) common to both studies was also robust ($r = 0.94$, $p < 0.0001$). Similarly, the correlation was 0.96 ($p < 0.0001$) for both the region weights and the subject scores for the second structure which was markedly abnormal in MD in both studies. The fourth structure obtained here mainly involved patterns of asymmetry in selective frontal and parietal regions. This corresponded to the third structure in our prior study with correlations of 0.74 and 0.81 for region weights and subject scores, respectively ($p < 0.0001$).

These findings demonstrated strong stability for SSM's blind determination of topographic effects, despite reducing the number of MD and normal subjects and introducing AD patients. Most critically, these findings indicate that the third topographic structure (GIS3) identified here is a new regional pattern that emerged due to the inclusion of AD patients. This pattern is not characteristic of normal controls or MD. Since this parietotemporal network is only manifested with the inclusion of AD patients, it is the most likely to reflect the primary pathophysiology of this condition. Nonetheless, the AD group was also abnormal in manifesting the remaining three patterns. This indicated that, in addition to being characterized by a parietotemporal deficit, AD alters the expression of regional patterns that are characteristic of normal functioning. To our knowledge, the serial analytic approach exemplified here

(two group analysis followed by three group analysis) represents the first attempt to distinguish when an illness produces abnormalities in normal patterns of brain region interaction and where an illness imposes new patterning.

Clinical Correlates of Global and Topographic Deficits

The relationships within the AD group between illness severity and CBF parameters were determined. The clinical indices were mMMS and BDRS scores, duration of illness and age at AD onset. The CBF parameters were raw global CBF, the GSF and scores on the four topographic structures (SSFs). The clinical measures were used as predictors, together with PCO_2 values, in multiple regression analyses on each CBF parameter (Table 4). Separate analyses were conducted for the mMMS and BDRS. Patients with greater cognitive impairment (lower mMMS scores) had lower global flow. There were particularly strong relations between mMMS scores and scores on the third topographic structure, the network introduced by the AD sample. Patients with greater cognitive impairment had a more severe parietotemporal deficit. Patients with longer duration of AD had more abnormal scores on the first topographic structure, suggesting that at longer illness duration the degree of posterior flow deficit and relative 'hyperfrontality' increased. As with the mMMS, higher BDRS scores (indicating greater impairment in activities of daily life) were associated with lower raw global CBF and lower GSF. However, unlike the mMMS, the BDRS had weak relations with topographic deficits.

In our previous report (47), we found that older MD patients and those with greater symptomatic severity, as assessed by the HRSD, were more abnormal on the second topographic structure (the regional pattern associated with depressive illness). In the subsample of MD patients included here, the relationship between HRSD (mean ± s.d., $32.53 ± 7.63$) and SSF2 scores was maintained ($r = 0.37$, $p < 0.05$). However, possibly due to the restricted age range needed for group matching, there was no longer a relationship between MD patient age and SSF2 scores ($r = -0.06$, ns). The mMMS was administered to 16 of the 30 MD patients. As expected, MD patients, although scoring in an impaired range, had considerably higher mMMS scores ($46.31 ± 6.46$, range 33–53) than the AD group ($p = 0.0002$). Within the MD group, there were no relationships between mMMS scores and any of the four topographic profiles. Compared to the AD group, the range and variability in mMMS scores was reduced in the MD group. Nonetheless, the association between cognitive impairment and scores on the third topographic structure (SSF3) appeared to be specific to the AD group.

Comparison of SSM to a Conventional Statistical Approach

To contrast the findings with SSM, a conventional multivariate analysis was conducted as described in the Appendix. The MANCOVA on the 32 ratio scores yielded a significant group by region interaction ($p < 0.01$). Two linear discriminant functions that maximized group sepa-

TABLE 4
Relations in Alzheimer's Disease between Measures of Illness Severity and CBF Parameters

Variable	Global CBF b	GSF b	SSF1 b	SSF2 b	SSF3 b	SSF4 b
mMMS	0.48[†]	0.39[*]	−0.24	−0.17	0.65[§]	−0.15
BDRS	−0.45[†]	−0.41[†]	−0.13	0.05	−0.28	0.09
Duration of illness	0.09	0.08	−0.52[†]	−0.06	0.10	0.15
Age at onset	0.04	−0.08	−0.02	0.31	0.01	0.18
PCO_2	0.46[‡]	0.48[‡]	0.23	0.03	−0.01	0.03

[*]$p < 0.10$.
[†]$p < 0.05$.
[‡]$p < 0.01$.
[§]$p < 0.005$.
b = the standardized coefficient in the multiple regression of the clinical variables on each CBF parameter; mMMS = score on the modified Mini Mental State examination; and BDRS = the Blessed Dementia Rating Scale.

ration in regional patterns were obtained and subjects were scored for their manifestation of these regional profiles. The groups differed in manifesting each of the profiles ($p < 0.0001$). For the first structure, normals scored significantly higher than the MD group ($p < 0.0001$), who in turn scored higher than the AD group ($p < 0.0002$). Only the MD group was abnormal in the second pattern, differing from both controls and AD patients ($p < 0.0001$).

Table 5 presents the results of regression analyses examining the relationship between subjects' scores on the four SSM topographic structures (SSFs) and their scores on the two discriminant functions. Scores on each of the four SSM patterns were significantly associated with scores on the two discriminant patterns. To maximize group separation, the conventional approach had combined elements of the more discrete SSM patterns. This was supported by examination of the regional weights in the discriminant functions. For the first function, the correlations between these structure coefficients (z-transformed) and the region weights for the four GISs were 0.54, 0.43, 0.53 and 0.33, respectively ($0.06 \geq p < 0.002$). For the second function, the correlations were 0.54 ($p = 0.001$), −0.63 ($p = 0.0001$), 0.18 (ns) and 0.33 ($p = 0.06$), respectively. These analysis indicated that the topographic patterns detailed by the discriminant function were an amalgam of the more discrete networks revealed by SSM.

The discriminant function patterns showed relatively poor stability. In the previous study restricted to MD and normal controls, a single discriminant function was obtained. The region weights for this earlier pattern correlated 0.53 and −0.53 ($p = 0.002$) with the weights on the two functions obtained here. For subject scores on these patterns, the correlations were 0.74 and −0.53 ($p < 0.0001$). Validity was tested by examining the relationship of subject scores on the two discriminant patterns and the

mMMS, BDRS, duration of illness and age at onset values within the AD group. No significant effects emerged. The first discriminant pattern, detailed by the conventional multivariate approach as sensitive to AD, departed from classic descriptions of the parietotemporal deficit. In line with these descriptions, this pattern reflected bilateral parietal CBF reductions with preservation in primary sensory and motor areas. However, it also included a flow deficit in a right-sided prefrontal region with relative flow elevations in a bilateral anterior temporal region and a right-sided posterior parietal region. Part of the difficulty encountered by the conventional approach was due to poor separation of global and topographic effects. Despite being derived from analysis of ratio scores (normalization by the global mean), there was still a substantial correlation between scores on the first function and global CBF ($r = 0.49$, $p < 0.0001$).

As another comparative test of both approaches within the AD group, correlations were examined for each brain region between CBF values and mMMS scores. In one set of analyses, the regional values were normalized by the GSF with SSM's measure of global flow stripped of the influence of topographic effects. In a second set of analyses, the regional values were normalized by the raw global mean. In both analyses, bilaterally averaged CBF values were used to reduce the number of correlations performed. Figure 3 presents the findings. With GSF normalization, trends or statistical significance ($p < 0.1$) was obtained for six correlations (1.6 expected by chance, assuming independence). These effects uniformly indicated that greater cognitive impairment was associated with reduced regional CBF in parietotemporal cortex. With normalization by the raw global mean, five effects were obtained. Contrary to intuition, three of these correlations reflected inverse relations between mMMS scores and regional CBF values. The involved regions corresponded to areas thought to be least compromised by AD (15–19). In this light, the elevated ratio values at these regions were due to reductions of global CBF in AD patients who had marked topographic deficits in other brain areas. Further, with normalization by the raw global mean, only two parietal

TABLE 5
Relations between Scores on Four SSM Topographic Structures and Scores on the Two Descriptive Discriminant Functions

Variable	First discriminant function b	p	Second discriminant function b	p
SSF1	0.33	0.0001	0.28	0.001
SSF2	0.44	0.0001	−0.47	0.0001
SSF3	0.40	0.0001	0.15	0.08
SSF4	0.31	0.0001	0.31	0.0004

b = the standardized beta coefficient (df = 1, 85) in the multiple regression of the SSFs on discriminant function scores.
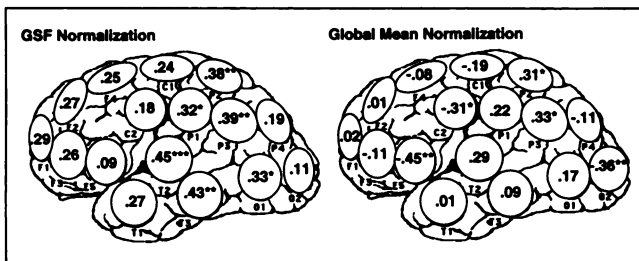
FIGURE 3. (Left) Correlations in Alzheimer's patients between bilaterally averaged regional CBF values normalized by the GSF and scores on the modified Mini Mental State examination. Significant correlations indicate that greater cognitive impairment was associated with lower blood flow. These effects occurred in the parietotemporal cortex. (Right) Correlations using the raw global mean for normalization. This normalization resulted in a scattered pattern, with greater cognitive impairment being associated with higher blood flow in three regions. These regions are traditionally thought to be least affected by AD. *$p < 0.10$; **$p < 0.05$; ***$p < 0.01$.

regions had positive associations between mMMS scores and CBF values, and these effects were marginal ($p < 0.1$). The contribution of the parietotemporal deficit to global mean values reduced the magnitude of positive associations within the topographic distribution of this deficit and artificially created negative associations in areas minimally compromised by AD.

The utility of each method for diagnostic classification was also examined. For SSM, scores on the four SSFs and the GSF were submitted to a discriminant classification analysis, predicting membership in the three groups. In a similar classification analysis, subject scores on the two descriptive discriminant functions and the global mean CBF served as predictors. As seen in Table 6, classification accuracy clearly exceeded chance (33%) with both sets of predictors ($p < 0.0001$), but classification accuracy was far from perfect. Overall, 66.7% of the subjects were correctly classified using the SSM indices and 75.6% were correctly classified using the measures derived with the conventional multivariate approach. Despite the fact that the conventional approach was not blind to group membership and had optimized group separation when deriving the topographic measures, the two methods were relatively comparable when used for classification purposes.

DISCUSSION

The MD and AD groups had marked and equivalent global CBF reductions. Global deficits in CBF and metabolism frequently have been noted in AD (*11-14*) but less consistently in MD (*30-39,46*). The equivalence of the clinical groups in global deficits may have been related to our concentration on elderly MD patients with severe depressive symptoms and AD patients with relatively short disease duration and mild to moderate cognitive impairment.

In both the MD and AD groups, the reductions in raw global CBF were partly due to topographic deficits. Consequently, the abnormalities in GSF, SSM's measure of region-independent global CBF, were smaller in magnitude. Nonetheless, both clinical samples had reduced GSF. This suggests that in addition to the processes that disrupt regional patterns, both conditions are characterized by a disturbance that reduces CBF across the cortex. The latter may involve dysfunction in subcortical nuclei with widespread cortical projection (*65,66*). In the AD group, the deficits in raw global CBF and in GSF covaried with the degree of cognitive impairment and of functional incapacity.

The primary aim of this study was to determine whether MD and AD could be distinguished in topographic deficits. Using either SSM or conventional statistical techniques, such specificity was established. We had previously identified an abnormal regional network in MD and showed that the extent of its abnormality correlated with the severity of depressive symptoms (*47*). These earlier findings were unaltered in this study and SSM parameters, derived blind to group membership, showed strong stability despite including a large AD group. By SSM, the regional abnormalities in MD are due to CBF reductions in a network comprising selective frontal, central, superior temporal and anterior parietal regions. This may correspond to the parallel distributed network involving strong reciprocal connectivity between polymodal association areas in prefrontal cortex and the inferior parietal lobule and the superior temporal sulcus (*41,42,67*).

A new topographic structure emerged with the inclusion of the AD group. Only the AD group was abnormal in manifesting this pattern, which corresponded closely to

TABLE 6
Agreement Between Discriminant Classification Based on CBF Parameters and Clinical Diagnosis

Discriminant classification	SSM parameters			Discriminant function parameters		
	Clinical diagnosis			Clinical diagnosis		
	Normal control	Depressed	Alzheimer's disease	Normal control	Depressed	Alzheimer's disease
Normal control	25	7	6	29	7	4
Depressed	5	20	9	1	18	5
Alzheimer's disease	0	3	15	0	5	21

Two predictive discriminant analyses were conducted classifying subjects as normal controls, depressed patients or as AD patients. One analysis used the four SSF scores and the GSF for classification. The other model used subject scores on the two descriptive discriminant functions and global mean CBF. The values indicate the number of subjects assigned to a particular group in each analysis as a function of their clinical diagnosis.

classic descriptions of the parietotemporal AD deficit (15–19). In support of this was the extent of cognitive impairment in AD that correlated strongly with the degree of abnormality in this network. These findings indicated that the abnormal parietotemporal topography in AD does not reflect disruption of a regional pattern intrinsic to normal functioning. Rather, it is due to AD imposing a new pattern of covariance on parietotemporal brain regions.

The AD group was also abnormal in manifesting the other three regional patterns previously identified in the study restricted to normal controls and MD patients. The parietotemporal deficit in AD would be expected to disrupt normal patterns of regional interaction in networks that include the parietotemporal cortex. Specifically, due to reduced CBF in these posterior regions, the AD group had exaggerated 'hyperfrontality,' thereby showing enhanced manifestation of the first SSM network that described an anterior-posterior dimension. The parietotemporal deficit partially overlapped with the regional abnormalities associated with MD. Both clinical conditions were associated with superior temporal and anterior parietal CBF reductions. This, and the fact that some AD patients may also have had compromised frontal regions, resulted in abnormal manifestation in the AD group of the second regional profile. Finally, others have shown that the parietotemporal deficit is variably expressed to a greater extent in the left or right hemisphere in a substantial number of AD patients (27–29). This likely accounted for why the AD group was disturbed in the fourth topographic profile which described normal patterns of asymmetry in frontal and parietal regions.

In future work, it may prove helpful to make this distinction between a disease introducing a new organization of interactions among brain regions and a disease secondarily disrupting normal patterns. The identification of new regional patterning should be of greater relevance for determining pathophysiology and, perhaps, etiology. For example, although the cause of the AD parietotemporal deficit in CBF and metabolism is still unknown, it is noteworthy that its regional distribution has considerable overlap with the cortical areas with the greatest density of histopathological abnormalities, including large neuron loss, neuritic plaques and neurofibrillary tangles (68–70). In contrast, secondary disruptions of regional networks present in normal functioning may be of importance in accounting for associated symptoms including patterns of behavioral disturbance. The findings also demonstrate that diseases may be multidimensional in altering patterns of regional interaction. This multidimensionality suggests that, for purposes of differential diagnosis, simple visual inspection of brain images may have critical limitations. In addition, the widely distributed nature of the abnormal network in MD makes its visual identification difficult.

In this study, the use of conventional multivariate statistical techniques also indicated that the MD and AD groups had distinct topographic abnormalities. However, limitations were identified in the application of these tech-

niques to complex imaging data. In our previous report, we concentrated on the problem such techniques have in separating topographic from global effects (47,48). This confounding of global and topographic effects occurred when using both raw or normalized values as dependent measures (47). Likewise in this study, despite use of the raw global mean to normalize regional values, there was considerable contamination of regional and global effects. Specifically, this contamination distorted the topographic profiles yielded by the descriptive discriminant analysis. It also obscured the relationships in the AD group between regional CBF values and the degree of cognitive impairment, thus producing some statistically significant, but clearly artifactual, effects. The findings of this three-group study also illustrate additional limitations. Discriminant analysis, as used here, is designed to yield the smallest number of topographic profiles that simultaneously maximize group separation (71,72). Consequently, intrinsic topographic dimensions on which groups do not differ cannot be identified. Group differences on independent topographic dimensions may be combined into a single regional profile or, conversely, an intrinsic regional pattern may be disjointedly represented as separate topographic dimensions to achieve better group separation. These methodological concerns were underscored by the findings regarding the stability and the validity of the topographic profiles derived with the conventional multivariate approach. In contrast to SSM, the discriminant profile we had previously identified as distinguishing MD patients and normal controls showed poor stability with the introduction of a new clinical group. Also in contrast to SSM, neither of the discriminant profiles obtained in this study were associated with clinical indices in the AD group.

Although both SSM and the conventional approach indicated that on average there were marked global and topographic differences among the groups, there was still considerable overlap among the groups in the derived indices. Consequently, in the classification analyses, neither approach demonstrated strong utility for purposes of differential diagnosis. Part of the problem here may be related to the poor spatial resolution of the lateral probe technique. Since SPECT and PET offer superior spatial resolution as well as the capacity to image subcortical structures, the power of SSM to identify stable sets of complex regional networks and to score patients in manifesting these patterns should prove critical in future applications of these imaging modalities.

CONCLUSION

We found that patient groups with MD and AD had equivalent reductions in global cortical CBF, but distinct topographic abnormalities. A single regional pattern was abnormal in major depression and manifestation of this abnormality covaried with the severity of depressive symptoms. We provided evidence that AD imposes a new regional organization and that the severity of cognitive im-

pairment in AD correlates strongly with manifestation of this parietotemporal deficit. In addition, AD modulates the expression of the regional patterns characteristic of normal function, resulting in widespread patterns of abnormality. The capacity to identify distinct topographic profiles as being characteristic of MD and AD supports the possibility that with further development functional neuroimaging techniques may contribute to differential diagnosis in these conditions.

APPENDIX: STATISTICAL PROCEDURES

Evaluation of Group Matching and Global CBF Effects

The adequacy of matching across the three groups was assessed by conducting ANOVAs on the continuous matching variables with group and sex as between-subject factors and by a chi-square analysis on the distribution of gender. Global CBF parameters were computed as the mean of raw values across the 32 detectors. ANCOVAs were used to examine group differences in global cortical CBF with group and sex as between-subject factors and age and PCO_2 as covariates. To identify the nature of differences among the groups, protected t-tests on covariate-adjusted means were used for post hoc comparisons.

Scaled Subprofile Model

The mathematical properties of SSM and its statistical assumptions have been described elsewhere (48, 73). Conceptually, SSM posits that for each individual each regional CBF or metabolic value comprises three components. The first component is a diffuse or region-independent GSF that modulates or scales all regional values for a given individual. The GSF is similar to the mean CBF or CMR across brain regions, but the contributions of topographic patterns are removed in the calculation of GSF. The second component is the Group Mean Profile (GMP), which corresponds to the average topographic distribution manifested across a total sample. Ignoring differences that may pertain to subject groupings, this mean component is the best descriptor of the similarity across subjects in topography. The third component is the SRP and corresponds to the variability that is both subject and brain region dependent, that is, the regional pattern unique to each subject. Therefore, for each subject, j, and for each brain region, i, $rCBF_{ij}$ may be expressed as:

$$rCBF_{ij} = GSF_j \times GMP_i \times (1 + SRP_{ij}). \qquad Eq. 1$$

In clinical research applications of brain imaging, the topographic alterations produced by disease entities will be reflected in the SRP, the variability that is both subject (e.g., disease) and brain region specific. However, this source of variability is likely to be small when compared to the large individual differences in global values and the between-region variability associated with the average profile across individuals (47). For example, in the current study, a repeated measures ANOVA (diagnostic group [3 levels] by brain region [32 levels]) was conducted on the raw ISI values. The variability that was both subject- and region-dependent comprised only 12.5% of the total variability. A significant group by region interaction was obtained (p < 0.0001) indicating that the groups differed in topographic effects. However, the sum of squares associated with this interaction comprised only 5.6% of the subject by region variability and thus, only 0.7% of the total sum of squares. As a method of signal amplification, an SSM analysis begins by isolating the SRPs, thereby removing considerable extraneous variance.

SSM conceives of the SRPs as being composed of independent sets of topographic networks. These networks correspond to different patterns of covariance among brain regions. The contribution of a particular brain region to a network, that is, its importance in the covariance relationships within the pattern, is quantified by its weight on the corresponding GIS. Therefore, the GIS is a vector of regional values, representing the covariance relationships among brain regions. Furthermore, since different individuals manifest these relationships to greater or lesser extents, a SSF can be derived to capture the individual differences in manifesting each network. For each subject, j, brain region, i, and topographic network, k, the SRPs may be expressed as:

$$SRP_{ij} = \sum_{k=1}^{k} SSF_{kj} \times GIS_{ki}. \qquad Eq. 2$$

As indicated, SSM posits that variability in individual subject's raw global CBF or metabolic values across brain regions (CBF_j) are due to individual differences in both the region-independent GSF and in manifestation of topographic profiles (SSF_js). Once the SSFs are derived, the contributions of these individual differences in topography can be removed from the raw global means, resulting in computation of the GSF. In simplified form, this may be expressed as:

$$\ln(GSF_j) = \ln(CBF_j) - \sum_{k=1}^{k} B_k \times SSF_{kj} + B_0. \qquad Eq. 3$$

For each network, k, B_k is a constant corresponding to the beta coefficient in the linear regression of the SSF_js on CBF_j and B_0 corresponds to the intercept.

The procedural steps used to compute these parameters are as follows. All SSM indices are derived by applying the model to the data from the total sample, blind to group membership. In this study, the rCBF values of 90 subjects were submitted to the model. Natural logarithmic transformation is applied to the raw rCBF values at each brain region, allowing the multiplicative relations between GSF_j, GMP_i and SRP_{ij} (Equation 1) to be expressed additively. To produce the approximation of the SRPs (Equation 1), the mean value at each region, determined across the total sample ($rCBF_i$) and each subject's global mean value (CBF_j), were subtracted from each subject's regional values ($rCBF_{ij}$). Since GSF is unknown at this point, the global mean value (CBF_j) is used as an approximation. This subtraction procedure corresponds to removing the GMP and an approximation of the GSF from the regional values of each subject. Since these subtractions were performed after logarithmic transformation, the SRP values are similar to the ratio scores often used in conventional analyses where raw regional values are normalized by the subject's global mean.

After isolating the SRPs, the values are arranged so that columns correspond to subjects and rows correspond to brain regions and the between-subject profile covariance matrix is computed. A principal-components factor analysis (PCA) is performed on this SRP covariance matrix and a set of unrotated factors (eigenvectors) is extracted. The PCA iteratively extracts independent linear factors that maximally account for SRP variance. The weights on each factor quantify the extent to which each topographic pattern is manifested by each subject and correspond to the SSFs. By definition, the mean score of the total sample for each SSF is zero, indicating that SSF scores capture the relative and not absolute extent to which a topographic structure is

manifested. Using standard regression techniques, the loading of each brain region on each factor is also determined, providing a first approximation to the spatial representation of the network or GIS. The number of factors to retain is determined by applying the Scree test (73) to the set of factor eigenvalues and by examining the extent to which the SSFs account for the variance in global CBF values.

Following Equation 3, the SSFs are submitted to a simultaneous multiple regression analysis, predicting the global mean CBF values ($\ln[CBF_j]$). The GSF corresponds to the residual between predicted and obtained values. Adding the intercept term to the residuals and taking the antilog of this value produces the final form of the GSF in the original CBF units. The beta coefficient for each SSF_k from this regression characterizes the extent to which the particular topographic structure contributed to global mean values. These regression coefficients are added as a constant (or offset) to the region loadings of the respective GIS. This corrects for the distortion in region weights introduced by normalizing by the subjects' global mean values in the computation of SRPs. The standard error associated with each beta coefficient is used to establish confidence boundaries for each GIS in identifying the set of regions most critical in defining the topographic pattern. Thus, the variability in rCBF is partitioned so that each subject is scored in their manifestation of each one of a set of topographical profiles, as well as in their region-independent global CBF. In this study, to determine whether the groups differed in global flow (GSF) or topographic organization (SSFs), standard ANCOVA and MANCOVA procedures were applied.

Extension of Conventional Multivariate Statistical Approaches

We contrasted the findings from SSM with those obtained using conventional multivariate statistical techniques. Since SSM was designed to reveal independent sets of topographic patterns and to score individuals for the degree to which they manifested these networks, we developed methods that allow derivation of similar measures using a conventional multivariate approach. A MANCOVA (grouped by sex, with age and PCO_2 as covariates) was conducted on the CBF values at the 32 detectors. The aim was to establish a significant group by region interaction, thereby confirming that the groups differed in topographic effects. Based on the characteristic vectors (72), the descriptive discriminant functions that characterized this interaction were computed. These linear functions produce optimal weights for each brain region, maximizing separation of the groups in their overall means on the functions, i.e., the average topography within a group (71). Subject scores were derived for each discriminant function, quantifying the extent to which each subject manifested each topographic pattern. These subject scores were computed by multiplying the raw values at each brain region by the corresponding region weight and summing across regions. Once these subject scores were derived, Pearson product-moment correlations were computed across the sample between the raw values at each region and each subject's score on the respective discriminant function. These correlations quantified of the importance of individual regions to the group separation in topography. Such correlations, termed structure coefficients, are thought to be more stable than the original regional weights in the descriptive discriminant functions (71, 73). Standard significance tests of the correlations (structure coefficients) identified the sets of brain regions that defined the topographic patterns that distinguished the groups.

This application of a conventional multivariate approach was applied twice, using either the raw rCBF values at each detector or the raw values normalized by each subject's global mean (i.e., ratio scores) as dependent measures. Only the results using ratio scores are reported. The findings using the raw values were deemed less satisfactory for two reasons. First, as in our previous study (47), in the analysis of raw values, the linear discriminant functions that characterized the topographies that distinguished the groups were highly contaminated by the group differences in global CBF. This suppressed the topographic abnormalities in the clinical groups by saturating the structure coefficients with the global differences in CBF. Second, SSM's detailing of topography was based on analysis of normalized values (SRPs). Consequently, submitting ratio scores to the conventional statistical approach allowed for more even-handed comparison with SSM.

Comparison of Statistical Models

The reliability and validity of SSM and the conventional multivariate approach in detailing topographic abnormalities were evaluated. Both approaches had been applied in a previous study of 41 depressed patients and 40 controls (47). The sample examined here included 60 of the previous subjects (30 depressed and 30 controls) and 30 new patients with Alzheimer's disease. The stability of each method's detailing of topographic patterns and subject scores for these patterns was evaluated by testing reproducability in the subjects common to both studies. For SSM, correlation coefficients were computed between the regions loading on comparable GISs and for comparable SSFs. For the conventional approach, similar correlations were performed on the structure coefficients (after z-transformation) and on the subject scores on the discriminant functions.

Validity was assessed in several ways. The conventional approach yielded fewer topographic structures than SSM. To determine whether the topographies reflected in the discriminant functions were an amalgam of the more discrete SSM patterns, multiple regression analyses were conducted predicting the subject discriminant function on scores on the basis of the SSFs. Within the Alzheimer's sample, multiple regression analyses were also used to examine the relations between clinical indices of disease severity and each method's scoring of individual differences in topography. As an additional step, correlations were computed between extent of global cognitive deficit (MMS) and regional CBF values within the Alzheimer's sample. The regional values were normalized by either SSM's measure of region-independent global flow (GSF) or by the raw global mean. Finally, to explore utility for differential diagnosis, the parameters derived with both approaches were submitted to predictive discriminant classification analyses, using the topographic and global values to classify subjects into the three diagnostic groups. In these classification analyses, the prior probabilities reflected the sample size of each group, i.e., each group comprised 33.3% of all subjects. Throughout, ANCOVAs and MANCOVAs were performed using diagnostic group and sex as between-subject terms and age and PCO_2 as covariates. The significance of multivariate effects was assessed with the F-test associated with Wilks' λ. All effects were evaluated with two-tailed tests of significance.

REFERENCES

1. Liston EJJ. Occult presenile dementia. *J Nerv Ment Dis* 1977;164:263–267.
2. Wells CE. Differential diagnosis of Alzheimer's dementia: affective disorder. In: Reisberg B, ed. *Alzheimer's disease: the standard reference*. New York: The Free Press; 1983:193–197.
3. McKhann G, Drachman D, Folstein MF, Katzman R, Price D, Stadlan EM. Clinical diagnosis of Alzheimer's disease: report of the NINCDS-ADRDA work group under the auspices of the Department of Health and Human Services Task Force on Alzheimer's disease. *Neurology* 1984;34:939–944.
4. Sulkava R, Haltia M, Paetau A, Wikstrom J, Palo J. Accuracy of clinical diagnosis in primary degenerative dementia: correlation with neuropathological findings. *J Neurol Neurosurg Psychiatry* 1983;46:9–13.
5. Chui HC. Dementia. A review emphasizing clinicopathologic correlation and brain-behavior relationships. *Arch Neurol* 1989;46:806–814.
6. Folstein MF, McHugh PR. Dementia syndrome of depression. *Aging NY* 1978;7:87–93.
7. Sackeim HA, Steif BL. The neuropsychology of depression and mania. In: Georgotas A, Cancro R, eds. *Depression and mania*. New York: Elsevier; 1988:265–289.
8. Meyer JS. Cerebral blood flow: use in differential diagnosis of Alzheimer's disease. In: Reisberg B, ed. *Alzheimer's disease: the standard reference*. New York: The Free Press; 1983:267–277.
9. Holcomb HH, Links J, Smith C, Wong D. Positron emission tomography: measuring metabolic and neurochemical characteristics of the living human nervous system. In: Andreasen NC, ed. *Brain imaging: applications in psychiatry*. Washington, DC: American Psychiatric Press; 1989:235–370.
10. Guze BH, Baxter LR Jr, Schwartz JM, Szuba MP, Mazziotta JC, Phelps ME. Changes in glucose metabolism in dementia of the Alzheimer type compared with depression: a preliminary report. *Psychiatry Res Neuroimaging* 1991;40:195–202.
11. de Leon MJ, Ferris SH, George AE, et al. Positron emission tomographic studies of aging and Alzheimer disease. *AJNR* 1983;4:568–571.
12. Komatani A, Yamaguchi K, Sugai Y, et al. Assessment of demented patients by dynamic SPECT of inhaled xenon-133. *J Nucl Med* 1988;29:1621–1626.
13. Friedland RP, Jagust WJ, Huesman RH, et al. Regional cerebral glucose transport and utilization in Alzheimer's disease. *Neurology* 1989;39:1427–1434.
14. Small GW, Kuhl DE, Riege WH, et al. Cerebral glucose metabolic patterns in Alzheimer's disease: effect of gender and age at dementia onset. *Arch Gen Psychiatry* 1989;46:527–534.
15. Gustafson L, Risberg J. Regional cerebral blood flow measurements by the ^{133}Xe inhalation technique in differential diagnosis of dementia. *Acta Psychiatr Scand* 1979;60(Suppl 72):546–547.
16. Friedland RA, Budinger TF, Ganz E, et al. Regional cerebral metabolic alterations in dementia of the Alzheimer type: positron emission tomography with (^{18}F)fluorodeoxyglucose. *J Comput Assist Tomogr* 1983;7:590–598.
17. Foster NL, Chase TN, Mansi L, et al. Cortical abnormalities in Alzheimer's disease. *Ann Neurol* 1984;16:649–654.
18. Haxby JV, Duara R, Grady CL, Cutler NR, Rapoport SI. Relations between neuropsychological and cerebral metabolic asymmetries in early Alzheimer's disease. *J Cerebral Blood Flow Metab* 1985;5:193–200.
19. Hellman RS, Tikofsky RS, Collier BD, et al. Alzheimer disease: quantitative analysis of I-123-iodoamphetamine SPECT brain imaging. *Radiology* 1989;172:183–188.
20. Frackowiak RSJ, Pozzilli C, Legg NJ, et al. Regional cerebral oxygen supply and utilization in dementia: a clinical and physiological study with oxygen-15 and positron tomography. *Brain* 1981;104:753–778.
21. Benson DF, Kuhl DE, Hawkins RA, Phelps ME, Cummings JL, Tsai SY. The fluorodeoxyglucose ^{18}F scan in Alzheimer's disease and multi-infarct dementia. *Arch Neurol* 1983;40:711–714.
22. Jagust WJ, Reed BR, Seab JP, Budinger TF. Alzheimer's disease. Age at onset and single-photon emission computed tomographic patterns of regional cerebral blood flow. *Arch Neurol* 1990;47:628–633.
23. DeKosky ST, Shih WJ, Schmitt FA, Coupal J, Kirkpatrick C. Assessing utility of single photon emission computed tomography (SPECT) scan in Alzheimer disease: correlation with cognitive severity. *Alzheimer Dis Assoc Disord* 1990;4:14–23.
24. Goldenberg G, Podreka I, Suess E, Deecke L. The cerebral localization of neuropsychological impairment in Alzheimer's disease: a SPECT study. *J Neurol* 1989;236:131–138.
25. Duara R, Grady C, Haxby J, et al. Positron emission tomography in Alzheimer's disease. *Neurology* 1986;36:879–887.
26. Perani D, Di Piero V, Vallar G, Cappa S, Messa C, Bottini G. Technetium-99m HMPAO-SPECT study of regional cerebral perfusion in early Alzheimer's disease. *J Nucl Med* 1988;29:1507–1514.
27. Foster NL, Chase TN, Fedio P, Patronas NJ, Brooks RA, Di Chiro G. Alzheimer's disease: focal cortical changes shown by positron emission tomography. *Neurology* 1983;33:961–965.
28. Koss E, Friedland RP, Ober BA, Jagust WJ. Differences in lateral hemispheric asymmetries of glucose utilization between early- and late-onset Alzheimer-type dementia. *Am J Psychiatry* 1985;142:638–640.
29. Haxby JV, Grady CL, Koss E, Horwitz B, Heston L, Schapiro M. Longitudinal study of cerebral metabolic asymmetries and associated neuropsychological patterns in early dementia of the Alzheimer type. *Arch Neurol* 1990;47:753–760.
30. Mathew R, Meyer J, Francis D, Semchuk K, Mortel K, Claghorn J. Cerebral blood flow in depression. *Am J Psychiatry* 1980;137:1449–1450.
31. Baxter L, Phelps M, Maziotta J, et al. Cerebral metabolic rates for glucose in mood disorders. *Arch Gen Psychiatry* 1985;42:441–447.
32. Buchsbaum MS, Wu J, DeLisi LE, et al. Frontal cortex and basal ganglia metabolic rates assessed by positron emission tomography with (^{18}F)2-deoxyglucose in affective illness. *J Affective Disord* 1986;10:137–152.
33. Kishimoto H, Takazu O, Ohno S, et al. ^{11}C-glucose metabolism in manic and depressed patients. *Psychiatry Res* 1987;22:81–88.
34. Baxter LRJ, Schwartz JM, Phelps ME, et al. Reduction of prefrontal cortex glucose metabolism common to three types of depression. *Arch Gen Psychiatry* 1989;46:243–252.
35. Devous MS. Imaging brain function by single-photon emission computer tomography. In: Andreasen N, ed. *Brain imaging: applications in psychiatry*. Washington DC: American Psychiatric Press; 1989;147–234.
36. Reischies FM, Hedde J, Drochner R. Clinical correlates of cerebral blood flow in depression. *Psychiatry Res* 1989;29:323–326.
37. Silfverskiöld P, Risberg J. Regional cerebral blood flow in depression and mania. *Arch Gen Psychiatry* 1989;46:253–259.
38. Martinot J, Hardy P, Feline A, et al. Left prefrontal glucose hypometabolism in the depressed state: a confirmation. *Am J Psychiatry* 1990;147:1313–1317.
39. Austin MP, Dougall N, Ross M, et al. Single photon emission tomography with ^{99m}Tc-exametazime in major depression and the pattern of brain activity underlying the psychotic/neurotic continuum. *J Affect Disord* 1992; 26:31–43.
40. Geschwind N. Disconnexion syndromes in animals and man. *Brain* 1965; 88:273–294, 584–644.
41. Mesulam M. Patterns in behavioral neuroanatomy: association areas, the limbic system and hemispheric specialization. In: Mesulam M, ed. *Principles of behavioral neurology*. Philadelphia: FA Davis; 1985:1–70.
42. Goldman-Rakic P. Circuitry of the prefrontal cortex and the regulation of behavior by representational knowledge. In: Plum F, Mountcastle V, eds. *Handbook of physiology, Sec. 1: the nervous system, volume 5: Higher cortical function*. Bethesda, MD: American Physiology Society; 1987:373–417.
43. Gur RC, Reivich M. Cognitive task effects on hemispheric blood flow in humans: evidence for individual differences in hemispheric activation. *Brain Lang* 1980;9:78–92.
44. Weinberger D, Berman K, Zec R. Physiologic dysfunction of dorsolateral prefrontal cortex in schizophrenia: II. Regional cerebral blood flow evidence. *Arch Gen Psychiatry* 1986;43:114–124.
45. Buchsbaum M, DeLisi L, Holcomb H, et al. Anteroposterior gradients in cerebral glucose use in schizophrenia and affective disorders. *Arch Gen Psychiatry* 1984;41:1159–1166.
46. Gur RE, Skolnick B, Gur RC, et al. Brain function in psychiatric disorders. II. Regional cerebral blood flow in medicated unipolar depressives. *Arch Gen Psychiatry* 1984;41:695–699.
47. Sackeim HA, Prohovnik I, Moeller JR, et al. Regional cerebral blood flow in mood disorders: I. Comparison of major depressives and normal controls at rest. *Arch Gen Psychiatry* 1990;47:60–70.
48. Moeller J, Strother S, Sidtis J, Rottenberg D. Scaled subprofile model: a statistical approach to the analysis of functional patterns in positron emission tomographic data. *J Cereb Blood Flow Metab* 1987;7:649–658.
49. Mountcastle V. Brain systems for directed attention. *J R Soc Med* 1978;71: 14–27.
50. Mesulam M. A cortical network for directed attention and unilateral neglect. *Ann Neurol* 1981;10:309–325.
51. Posner M, Walker J, Friedrich F, Rafal R. Effects of parietal injury on covert orienting of visual attention. *J Neurosci* 1984;4:1863–1874.
52. Spitzer R, Endicott J, Robins E. *Research diagnostic criteria for a selected group of functional disorders*. New York: Biometrics Research Division, New York State Psychiatric Institute; 1977.

53. Endicott J, Spitzer R. A diagnostic interview: the schedule for affective disorders and schizophrenia. *Arch Gen Psychiatry* 1978;35:837–844.

54. Hamilton M. Development of a rating scale for primary depressive illness. *Br J Soc Clin Psychol* 1967;6:278–296.

55. Prohovnik I, Mayeux R, Sackeim HA, Smith G, Stern Y, Alderson PO. Cerebral perfusion as a diagnostic marker of early Alzheimer's disease. *Neurology* 1988;38:931–937.

56. Mayeux R, Stern Y, Rosen J, Leventhal J. Depression, intellectual impairment and Parkinson's disease. *Neurology* 1981;31:645–650.

57. Stern Y, Sano M, Paulson J, Mayeux R. Modified mini-mental state examination: validity and reliability. *Neurology* 1987;37(Suppl 1):179.

58. Blessed G, Tomlinson BE, Roth M. The association between quantitative measures of dementia and of senile change in the cerebral grey matter of elderly subjects. *Br J Psychiatry* 1968;114:797–811.

59. Prohovnik I. Data quality, integrity and interpretation. In: Knezevic S, Maximilian V, Mubrin Z, Prohovnik I, Wade J, eds. *Handbook of regional cerebral blood flow*. Hillsdale, NJ: Erlbaum; 1988:51–78.

60. Prohovnik I, Knudsen E, Risberg J. Accuracy of models and algorithms for determination of fast-compartment flow by noninvasive ^{133}Xe clearance. In: Magistretti P, ed. *Functional radionuclide imaging of the brain*. New York: Raven; 1983:87–115.

61. Obrist W, Wilkinson W, Wang H, Harel D. The noninvasive ^{133}Xe method: influence of the input function on computed rCBF values. In: Knezevic S, Maximilian V, Mubrin Z, Prohovnik I, Wade J, eds. *Handbook of regional cerebral blood flow*. Hillsdale, NJ: Erlbaum; 1988:37–50.

62. Prohovnik I, Knudsen E, Risberg J. Theoretical evaluation and simulation test of the initial slope index for noninvasive rCBF. In: Hartmann A, Hoyer S, eds. *Cerebral blood flow and metabolism measurement*. Berlin: Springer-Verlag; 1985:56–60.

63. Prohovnik I, Smith G, Sackeim HA, Mayeux R, Stern Y. Gray-matter degeneration in presenile Alzheimer's disease. *Ann Neurol* 1989;25:117–124.

64. Meltzer CC, Leal JP, Mayberg HS, Wagner HNJ, Frost JJ. Correction of PET data for partial volume effects in human cerebral cortex by MR imaging. *J Comput Assist Tomogr* 1990;14:561–570.

65. Mesulam M, Mufson E, Levey A, Wainer B. Cholinergic innervation of cortex by the basal forebrain: cytochemistry and cortical connections of the septal area, diagonal band nuclei, nucleus basalis (substantia innominata) and hypothalamus in the rhesus monkey. *J Comp Neurol* 1983;214:170–197.

66. Metter E, Riege W, Kuhl D, Phelps M. Cerebral metabolic relationships for selected brain regions in healthy adults. *J Cereb Blood Flow Metab* 1984; 4:1–7.

67. Seltzer B, Pandya D. Afferent cortical connections and architectonics of the superior temporal sulcus and surrounding cortex in the rhesus monkey. *Brain Res* 1978;149:1–24.

68. Brun A, Englund E. Regional pattern of degeneration in Alzheimer's disease: neuronal loss and histopathological grading. *Histopathology* 1981;5: 549–564.

69. Pearson RCA, Esiri MM, Hiorns RW, Wilcock GK, Powell TPS. Anatomical correlates of the distribution of pathological changes in the neocortex in Alzheimer's disease. *Proc Natl Acad Sci USA* 1985;82:4531–4534.

70. Rogers J, Morrison JH. Quantitative morphology and regional and laminar distributions of senile plaques in Alzheimer's disease. *J Neurosci* 1985;5: 2801–2808.

71. Huberty C. Issues in the use and interpretation of discriminant analysis. *Psychol Bull* 1984;95:156–171.

72. Anderson TW. *An introduction to multivariate statistical analysis*. New York: Wiley; 1984.

73. Moeller JR, Strother SC. A regional covariance approach to the analysis of functional patterns in positron emission tomographic data. *J Cereb Blood Flow Metab*. 11:A121–A135.

74. Stevens J. *Applied multivariate statistics for the social sciences*. Hillsdale, NJ: Erlbaum; 1986.

EDITORIAL
Functional Brain Imaging in the Elderly

Alzheimer's disease (AD) and late-life depression (LLD) are usually thought of as discrete brain disorders. Unfortunately, as with many clinical syndromes, there can be considerable overlap in their presentation. Depressive disorders occur in 10%–20% of patients with AD (*1*), and some patients with LLD have cognitive deficits that reach clinically meaningful proportions (*2*) and may resolve with effective treatment of the underlying mood disorder (*3*). It is not surprising then that clinical diagnoses are not always reliable. One reviewer noted that 8% of British patients who were initially diagnosed with dementia were subsequently determined to have major depression (*4*).

For planning a therapeutic regimen, an accurate diagnostic assessment is critical. LLD is responsive to both an-

tidepressant medication and electroconvulsive therapy (ECT) (*5*). However, medication side effects are common in the elderly, who often have comorbid medical conditions, and medication-induced cognitive decline is especially likely in patients with dementia. ECT also generally worsens cognitive deficits, at least acutely, in all patients (*6*). A range of different treatment strategies has been proposed for patients with AD and several promising new agents are now being assessed in clinical trials (*7*). These medications also have side effects and their benefits are unlikely to be shared by patients with LLD.

Although progress in defining the pathophysiology of psychiatric disorders in the elderly has been slow, the available evidence clearly suggests that both LLD and AD are associated with derangements in brain structure and function. Structural brain imaging studies have shown that both disorders are associated with increased

rates of cerebral infarction, cortical atrophy and leukoencephalopathy (*8*). Similarly, functional brain imaging studies suggest that *global* cortical blood flow is decreased to a similar degree in patients with LLD or AD (*9,10*). Therefore, the development of brain imaging techniques with diagnostic utility for LLD and AD is likely to depend upon an assessment of alterations in *regional* brain metabolism either at rest or in response to pharmacologic challenge or neuropsychologic tasks.

In this issue of the *Journal*, Sackeim et al. (*11*) report an analysis of patterns of regional cerebral blood flow, determined using the ^{133}Xe inhalation technique, in large groups of well-matched patients with LLD and AD. A Scaled Subprofile Model (SSM), which was initially developed to identify abnormal functional networks in clinical brain images (*12*), was used to distinguish patient groups according to distinct topographic pro-

Regional Cerebral Blood Flow in Mood Disorders. II. Comparison of Major Depression and Alzheimer's Disease

Harold A. Sackeim, Isak Prohovnik, James R. Moeller, Richard Mayeux, Yaakov Stern and D. P. Devanand